Astron. Astrophys. 346, 313–321 (1999)

ASTRONOMY AND ASTROPHYSICS

Determination of solar cycle length variations using the continuous wavelet transform

M. Fligge[1], **S.K. Solanki**[1], **and J. Beer**[2]

[1] Institute of Astronomy, ETH-Zentrum, CH-8092 Zürich, Switzerland
[2] Swiss Federal Institute of Environmental Science and Technology (EAWAG), CH-8600 Dübendorf, Switzerland

Received 28 September 1998 / Accepted 23 March 1999

Abstract. The length of the sunspot cycle determined by Friis-Christensen & Lassen (1991) correlates well with indicators of terrestrial climate, but has been criticized as being subjective. In the present paper we present a more objective and general cycle-length determination. Objectivity is achieved by using the continuous wavelet transform based on Morlet wavelets and carrying out a careful error analysis. Greater generality comes from the application of this technique to different records of solar activity, e.g. sunspot number, sunspot area, plage area or ^{10}Be records. The use of different indicators allows us to track cycle length variations back to the 15th century. All activity indicators give cycle length records which agree with each other within the error bars, whereby the signal due to the solar cycle is weaker within ^{10}Be than in the other indicators.

In addition, all records exhibit cycle length variations which are, within the error bars, in accordance with the record originally proposed by Friis-Christensen & Lassen (1991). In the 16th century, however, the ^{10}Be record suggests a much longer cycle than the auroral record used by Friis-Christensen & Lassen. Also, the presence of a distinct 11-year cycle in the ^{10}Be record during the Maunder Minimum is confirmed. By combining the results from all the indicators a composite of the solar cycle length is constructed, which we expect to be more reliable than the length derived from individual records.

Key words: methods: data analysis – Sun: activity – Sun: solar-terrestrial relations – Sun: sunspots

1. Introduction

Studies aiming to uncover a possible solar influence on the Earth's climate system have often concentrated on searching for relations between indicators of solar activity and terrestrial climate records. In addition to searching for the prominent solar activity period of about 11 years in climate records a number of researchers have considered longer time scales. Friis-Christensen & Lassen (1991; henceforth referred to as FL91) were the first to point out that an extraordinarily high correlation exists between the length of the sunspot cycle and the northern hemisphere terrestrial temperature record. In this initial paper they considered the period 1861 to 1989. In a later paper Lassen & Friis-Christensen (1995) extended the cycle length record into the more distant past using a combination of sunspot number and auroral observations. They again find a good correlation between cycle length and indicators of climate. This result was further buttressed by observations of sun-like stars evaluated by Baliunas & Soon (1995) which revealed a close relationship between the length of stellar activity cycles and Ca II H & K emission flux, an indicator of stellar photometric brightness changes.

However, the goodness of the correspondence between cycle length and climate depends on the way the solar cycle length is determined and on the amount of smoothing applied to the cycle length record, as pointed out by Kelly & Wigley (1992). They called into question the conclusions of FL91, pointing out that the cycle length determined from the cycle maxima differs from that determined from minima. Also, different amounts of smoothing give widely different results. It is *a priori* unclear which one of the different possible cycle length records is the one to use.

The present paper addresses this question by determining the evolution of the cycle length via a robust and "objective" technique, namely the wavelet transform. A wavelet analysis does not rely on determining exactly when maxima and minima of activity occur (which can depend strongly on the type of record analyzed, e.g., daily, weekly, monthly or yearly means). Also, the whole data set enters into the wavelet analysis and not just relatively few points near the maximum and minimum.

We also consider two other questions. The first is how representative is the length of the sunspot number cycle analyzed by FL91, Kelly & Wigley (1992) and others? We address it by applying the wavelet transform also to other indicators of solar activity besides the sunspot number. Finally, we consider the possibility of determining the length of the sunspot cycle also in the pre-telescopic period, at times when no reliable direct observations of solar activity indicators were made. We explore this period by analyzing the ^{10}Be concentration record obtained from Greenland ice cores. The application of wavelets to ^{10}Be also provides an independent test of the finding of Beer et al. (1998) that the solar activity cycle persisted also during the

Send offprint requests to: M. Fligge

Maunder Minimum, which they obtained using Fourier techniques.

Wavelet-based analysis techniques have been applied to a variety of astronomical problems (e.g., Hjorth et al. 1992, Starck et al. 1995) including studies of solar cycle variability (Vigouroux & Delache 1993, 1994; Ochadlick et al. 1993). In the present paper we make use of the continuous wavelet transform which is particularly suited for time-frequency studies of non-stationary signals such as records of solar ac tivity. Unlike the Fourier transform it not only provides informati on on the time-averaged frequencies present in the signal, but also allows the instantaneous power to be determined in the various frequencies.

Ochadlick et al. (1993) first used the wavelet transform to determine the solar cycle length from the sunspot relative number record. Frick et al. (1997) later applied the same technique to an extended record of solar activity, the so-called group sunspot numbers (Hoyt et al. 1994).

Our work differs from these investigations in several ways. Firstly, we investi gate different indicators of solar activity instead of just a single record (e.g. Zürich sunspot relative numbers, group sunspot numbers, sunspot areas, facular and plage areas, etc.). This allows us to test if the length of the solar activity cycle is a robust parameter that is almost independent of the employed indicator. Also, facular and plage indicators serve as proxies of a different part of the solar magnetic field than sunspots. In addition faculae influence the brightness of the Sun in a different way from sunspots. It is therefore important to know whether the length of the facular cycle is identical to that of the sunspot cycle.

Secondly, we carry out a careful error analysis (based on the work of Starck & Bijaoui, 1994 and Torrence & Compo, 1998). This allows us to compare quantitatively the cycle length variations resulting from the different indicators with each other and with the cycle length determined by FL91. As in the case of Fourier analysis a careful error estimate is essential for the identification and proper interpretation of significant features in a wavelet power spectrum.

Thirdly, we include the long-term record of ^{10}Be (Beer et al. 1994a) which offers the possibility of tracking variations of the cycle length back to the beginning of the 15th century, i.e. over almost 600 years. Finally, we combine the suitably weighted cycle lengths resulting from the various indicators into a single record.

In Sect. 2 we give an overview of the investigated time-series of solar activity indicators and point out their advantages and shortcomings. We briefly introduce the continuous wavelet transform and sketch some of the relevant properties of the Morlet wavelets used here in Sect. 3. In Sect. 4 we describe the analysis of the five direct solar activity records, emphasize some peculiarities and discuss the resulting wavelet power spectra and the corresponding solar cycle length variations. The findings for the ^{10}Be record are presented separately in Sect. 5. In Sect. 6 we present a composite solar cycle length record covering almost 600 years. Finally, we summarize our conclusions in Sect. 7.

2. Indicators of solar activity

Solar activity is strongly variable, subject to a cyclic behavior with a period of about 11 years that is driven by the global evolution of the Sun's magnetic field. Its surface manifestations, like sunspots or faculae, influence the solar brightness which changes in phase with the global solar activity. Sunspots have been regularly recorded ever since the invention of the telescope at the beginning of the 17th century. Regular observations of faculae, however, started much later since they are far less clearly visible in white light. These records represent the only direct observations of past solar variability. Cosmogenic isotopes, however, provide indirect measures. They have the advantage that their records also reach back to pre-telescopic times.

In the present paper we use three different recordings of sunspot properties. Firstly, we employ Zürich sunspot relative number, $R_{\rm Z}$, introduced by Rudolf Wolf in the last century. It is obtained by counting the number of sunspots and sunspot groups present on the solar disc, combining them in an appropriate manner and weighting the result by an individual, observer-dependent, factor. Time-series of $R_{\rm Z}$ date back to the beginning of the 18th century. Secondly, we use the group sunspot number, $R_{\rm g}$, proposed by Hoyt et al. (1994) and Hoyt & Schatten (1998). It represents a revision of $R_{\rm Z}$ based on group counts alone and is extended by additional historical sources. $R_{\rm g}$ and $R_{\rm Z}$ differ mostly for the period before 1880. Thirdly, we analyze measurements of sunspot areas, A_s. The earliest regular recordings of sunspot areas date back to 1874 and were performed by the Royal Greenwich Observatory. Sunspot area measurements are much more susceptible to instrumentation, methodology and local observing conditions than sunspot number counts and time-series of different stations must be combined with great care. We employ the composite of sunspot area measurements proposed by Fligge & Solanki (1997).

Recording faculae and following their evolution proves to be much more difficult. In white light faculae show up only near the solar limb. Their contrast exhibits a strong center-to-limb variation and vanishes near disc-center. In addition, the highly scattered faculae have a much more complex morphology compared to sunspots. First regular recordings of photospheric white-light facular areas A_f were started, together with A_s measurements, in 1874, again by the Royal Greenwich Observatory. Observations ceased in 1976. We use their record as a proxy of facular behavior.

Plages, the chromospheric counterparts of faculae, are often used as a surrogate of faculae due to their pronounced contrast relative to the quiet Sun all over the solar disc. Plage measurements in the K-line of Ca II have been performed by the Mt. Wilson observatory between 1915 and 1984. They have been digitized and made available by Foukal (1996). We use this record of Ca plage area measurements, $A_{\rm p}$, as the fifth direct indicator of solar magnetic activity.

If solar variability is to be investigated for pre-telescopic times indirect indicators of solar activity and magnetism need to be used. Examining records of cosmogenic isotopes archived in tree rings (^{14}C) or Greenland ice-cores (^{10}Be) proves to be

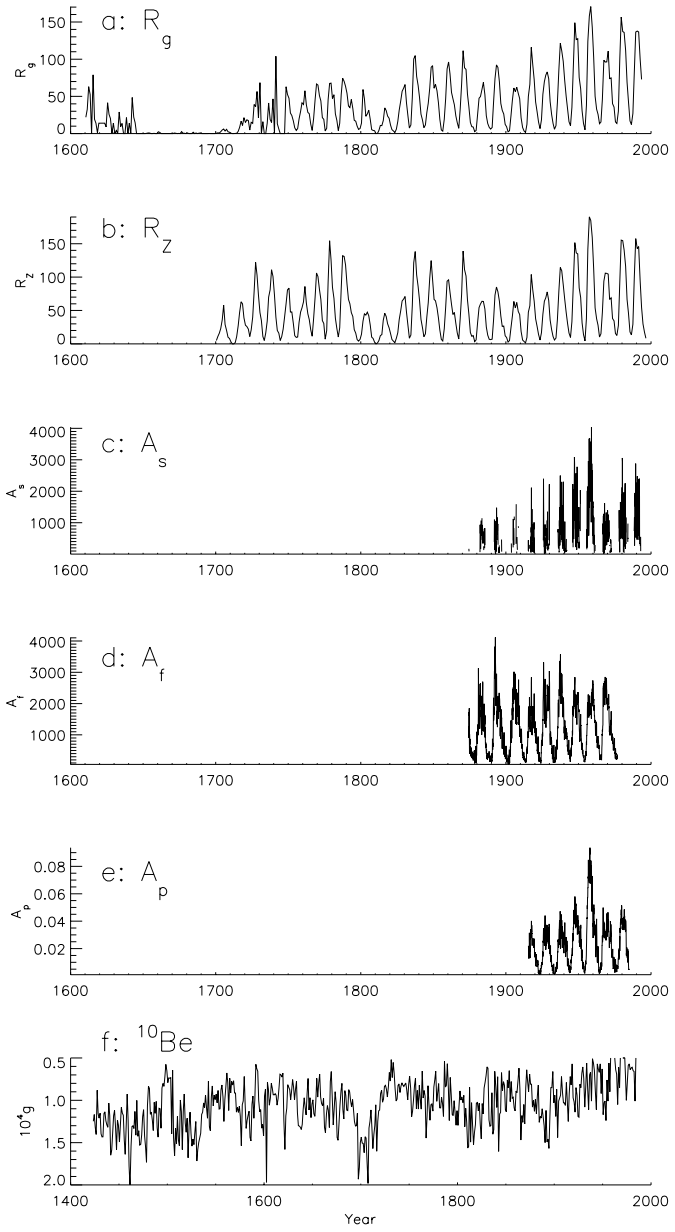

Fig. 1a–f. Indicators of solar magnetic activity. From *top* to *bottom*: **a** Group sunspot number, $R_{\rm g}$, **b** Zurich relative sunspot number, $R_{\rm Z}$, **c** Sunspot area, A_s, in parts-per-million (ppm) of the solar hemisphere, **d** Facular area, A_f, in ppm, **e** Ca plage area, $A_{\rm p}$, in fraction of the solar disc, and **f** ^{10}Be concentration measurements. Note that the ^{10}Be record is plotted upside down to account for the inverse relationship between ^{10}Be concentration and solar activity. Also, the horizontal scale for the ^{10}Be record is somewhat compressed relative to the rest. Together, these six proxies offer the possibility to study almost 600 years of the Sun's history.

fruitful. Cosmogenic isot opes are produced when cosmic rays hit the Earth's upper atmosphere, thereby interacting with atmospheric nitrogen or oxygen. The charged cosmic rays also interact with the solar wind and the solar magnetic field permeating interplanetary space, leading to an anti-correlation between solar activity and the production rate of cosmogenic isotopes. Thus, during times of high solar activity, when the Earth is better shielded from cosmic rays by the enhanced inter-planetary magnetic field, less isotopes are produced.

In the present study we use the ^{10}Be record from the Dye 3 ice core obtained in Greenland (Beer et al. 1990). This time-series is available back to the beginning of the 15th century. Hence it is about two centuries longer than any direct proxy. The mean residence time of ^{10}Be is about one year (Beer et al. 1994b). The annual resolution makes ^{10}Be particularly suitable for long-term studies of solar variability on time scale of the solar cycle. However, due to the short residence time, ^{10}Be is more susceptible to changes of local weather conditions than, e.g., ^{14}C measurements. This alters solar induced signatures within the ^{10}Be record.

We plot all indicators in Fig. 1. Panels a–e show the five direct indicators, i.e. a) group sunspot numbers ($R_{\rm g}$), b) Zürich sunspot numbers ($R_{\rm Z}$), c) sunspot areas (A_s), d) facular areas (A_f) and e) Ca plage areas (A_p). In panel f) we plot the ^{10}Be record. Note the reversed y-axis to account for the inverse relation between ^{10}Be and solar activity. For $R_{\rm Z}$, $R_{\rm g}$ and ^{10}Be we plot yearly values while A_s, A_f and A_p are given on a monthly basis.

3. The continuous wavelet transform

Fourier analysis decomposes a signal into different sines and cosines and provides information about how much of each frequency the signal contains. However, the uncertainty principle forbids the extraction of any temporal information from the Fourier transform since sines and cosines are described by a single, sharp frequency and, hence, cannot be localized in time at all.

Wavelet analysis overcomes this restriction using building blocks which are localized in both time and frequency. These building blocks or *wavelets* are characterized by two parameters, a and b, describing scale (frequency) and position in time, respectively. The wavelet transform, hence, also provides information on the temporal distribution of the frequencies and is, thus, naturally suited to localize frequency changes within the signal.

The coefficients of the wavelet transform are obtained by projecting the signal onto the corresponding wavelet. For a detailed introduction into the subject see, e.g., Grossmann et al. (1993), Chui (1992) and references therein.

In Sect. 4 and 5 we investigate variations of the main period of a given solar activity proxy. We do this using the wavelet power spectrum, $P_f(a,b)$, which is, in full analogy to the power spectrum used in Fourier analysis, given by the square of the wavelet coefficients. Following Goupil et al. (1991) we also calculate the global wavelet power spectrum by averaging the wavelet power spectrum over time.

The subsequent analysis is based on Morlet wavelets plotted in Fig. 2. Corresponding to damped harmonics these wavelets are well suited to analyze oscillatory signals (Grossmann & Morlet 1984).

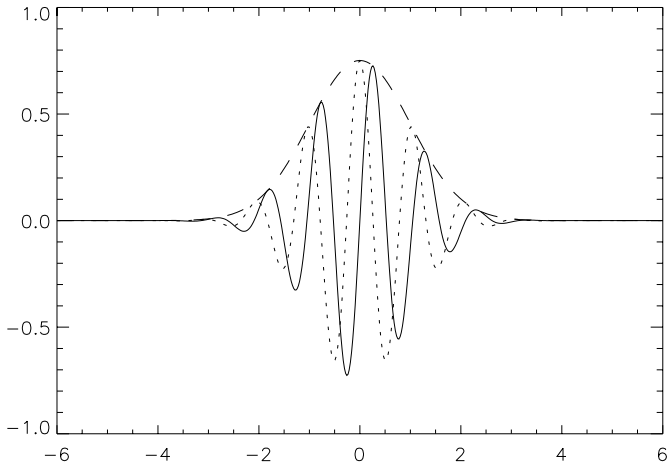

Fig. 2. The complex Morlet wavelet. Plotted is its real (solid) and imaginary (dotted) part as well as its absolute value (dashed). The real and imaginary part of the Morlet wavelet corresponds to a cosine or sine, respectively, multiplied with a Gaussian.

In fact, the Morlet wavelets have infinite support. However, they can be considered to vanish outside a certain interval since they fall off rapidly enough. In practical applications one is dealing with signals of finite length. Consequently, the wavelet transform is biased near the signal's boundaries. Since the analyzing wavelet gets broader with increasing scale a more wavelet coefficients are biased when going to larger and larger scales. This is described by the so-called domain-of-influence (DOI; Grossmann et al. 1993) which is defined by the width of the analyzing wavelet. Coefficients lying within the DOI are less reliable.

The transformation of the wavelet scale a into the more familiar Fourier period T is carried out following Meyers et al. (1993).

3.1. Determination of the level of confidence

Assume a signal composed entirely of Gaussian distributed noise with a variance of σ^2. The wavelet power spectrum $P_{noise}(a,b)$ of such a signal follows a χ^2 distribution (Starck & Bijaoui 1994) in full analogy to the Fourier power spectrum. In the case of the Morlet wavelets, which are complex, the distribution has two degrees of freedom, i.e. $P_f(a,b)$ is distributed as (Torrence & Compo 1998)

$$P_{noise} \Rightarrow \frac{1}{2}\sigma^2\chi^2_2. \quad (1)$$

From this, levels of confidence can be calculated which indicate the probability that a given coefficient of the wavelet power spectrum is real and not due to noise. Usually, we use a 95% confidence level to separate the signal from its background noise.

Neighboring wavelet coefficients are not uncorrelated, neither in time nor in scale, but are linked to each other by the width of the analyzing wavelet. This decreases the degree of freedom of the global wavelet power spectrum with increasing scale. Therefore, also the level of confidence depends on scale a. Again, we use the results of Torrence & Compo (1998) for the error estimation of global wavelet power spectra.

4. Analysis of direct solar activity records

We now apply the continuous wavelet transform to the investigation of solar activity records. All the transforms discussed here were carried out using 96 scales, i.e. 4 octaves with 24 voices each. They cover the periods between 2 and 32 years.

In Fig. 3 we present contours of wavelet power of the time-series of yearly values of R_Z as a function of time (x-axis) and period (y-axis). The wavelet power spectrum of monthly values is practically identical.

In agreement with time series of all the investigated direct indicators (see below), the ridge around the 11 years activity period is very strong and highly significant as indicated by the 95% confidence level. The wavelet power is strongest during the last 50 years as expected for the high mean level of activity of the present Sun. The curved lines stretching across both boundary regions of the wavelet power spectrum mark the the appropriate DOI.

A similar picture is found for the sunspot areas A_s whose wavelet power spectrum is plotted in Fig. 4 (based on monthly values). Since the time period for this record is significantly shorter than for R_Z a larger part of the wavelet power spectrum is biased. To check the influence of the signal's sampling rate on the wavelet power spectrum we also used yearly means of A_s and found no significant differences within the analyzed range of periods except that, due to the lower sampling rate, the significance of the ridge around the 11 years activity period is decreased.

As expected, examination of the global wavelet power spectrum reveals a very prominent peak around the 11-year period for all five direct proxies. As an example we present the global wavelet power spectrum of R_Z in Fig. 5. The peak corresponds to a mean period of 10.7 years for the analyzed interval, i.e. between 1700 and the present. Evaluation of the global wavelet power spectrum for the other four proxies gives similar mean periods with values between 10.5 – 10.7 years. The dashed line represents the 95% confidence level based on the noise level estimation described in Sect. 3.1. Note the considerable width of the main power peak. This is partly due to the variation of the cycle period as a function of time, but is partly also a result of the fact that due to the achievement of a certain time resolution, frequency resolution is reduced. Since the wavelet power peaks lie well above the noise and there is only a single peak around 11 years the period of its maximum can be determined with far greater accuracy than is suggested by its width.

4.1. Cycle length variations

After the wavelet power spectrum has been calculated the cycle length variations $C(t)$ of the solar activity proxies must be extracted. This is done following the ridge around the 11-year period of the wavelet power spectrum indicated by the thick lines in Figs. 3 and 4. To calculate $C(t)$ for a given time $t = b_0$

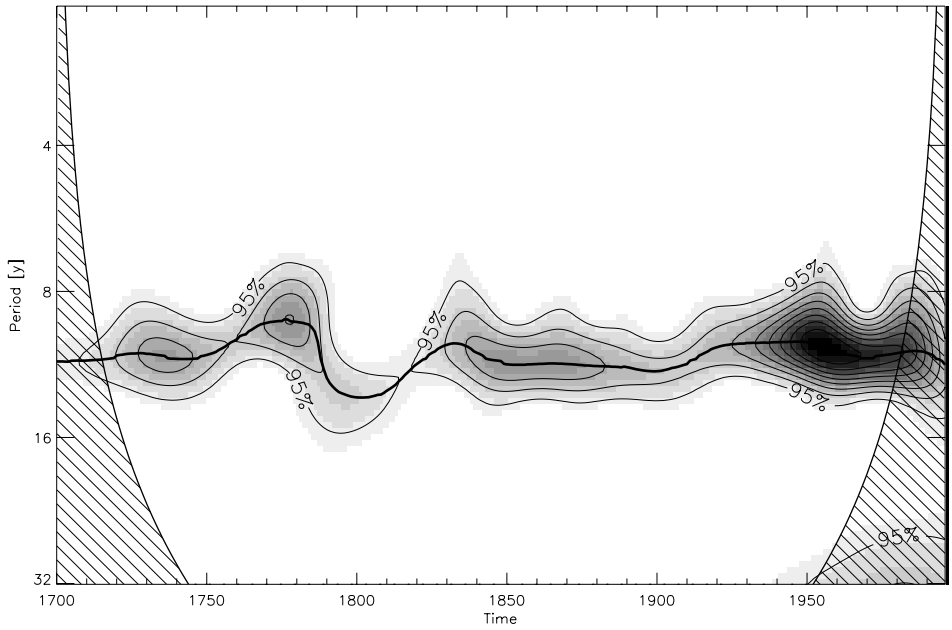

Fig. 3. Wavelet power spectrum of the record of sunspot relative numbers, R_Z, from 1700 to the present. Wavelet power is indicated by the contour lines. From left to right wavelet power spectra at different times are plotted. Marked is the contour line of the 95% confidence level. The other contours indicate increasingly larger significance of the wavelet power spectrum coefficients. The domain-of-influence is given by the hatched areas at both sides of the image (see Sect. 3). The solar activity ridge (thick line) is highly prominent and lies well above the noise level. The shading was chosen in order to emphasize the solar activity ridge and the significance of the power.

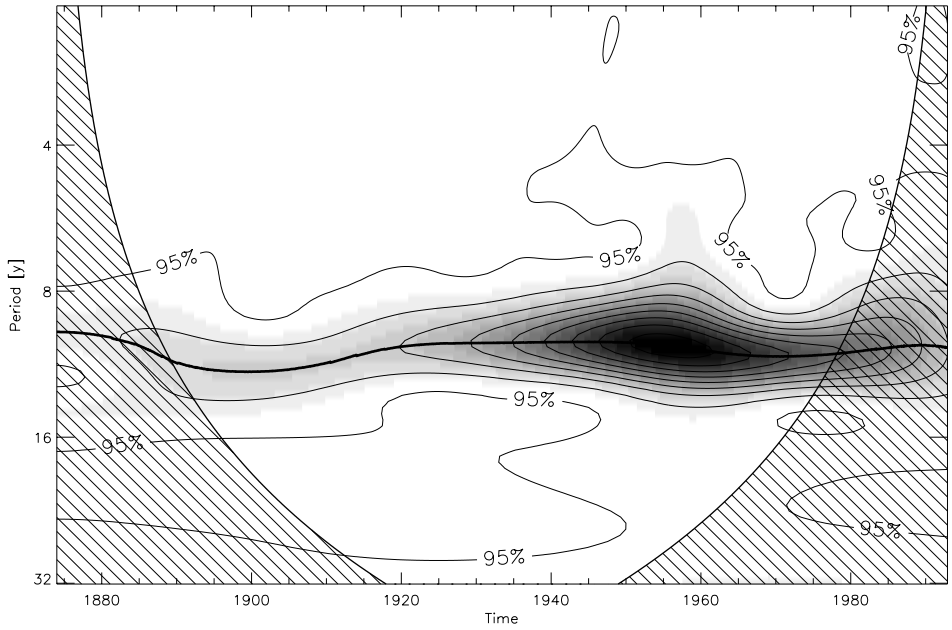

Fig. 4. Same as Fig. 3 but for the record of sunspot areas A_s. A larger fraction of the image lies within the DOI due to the smaller time base. Again, as for all direct indicators, the solar activity period is pronounced and highly significant.

we determine the local maximum of $P_f(a, b_0)$ (as a function of a) at $a \approx 11$ year by partial derivation. Note that for the five direct proxies this corresponds to finding the global maximum since the 11 years solar activity period is by far the most prominent one in those records. Ochadlick et al. (1993) used a somewhat different method based on the ridge analysis originally proposed by Delpart (1992). However, Frick et al. (1997) found no significant difference between the two methods as far as the extracted cycle length variations are concerned.

The results are presented as the solid curves in Fig. 6. Plotted are, from top to bottom, a) R_g, b) R_Z, c) A_s, d) A_f and e) A_p. Each proxy is plotted over the whole time period over which significant power has been found. In addition, we plot the record of cycle length variations derived by FL91 (dotted line in each panel) which can be used as a reference to mutually compare the different results. The error bars are plotted at times of solar activity minimum.

The accuracy of $C(t)$ is limited by the following factors: Firstly, by the spectral resolution of the analyzing wavelet. However, as already mentioned in the previous section the period of the maximum of the wavelet power spectrum around the 11 years activity ridge can be determined with much greater accuracy than is suggested by the width of the analyzing wavelets. Secondly, by the significance of the coefficients of $P_f(a, b)$ which decreases towards the boundaries of the signal. The influence of these two factors has been estimated empirically using artificial signals of different length. Thirdly, by the background noise inherent in each proxy record which can be estimated from

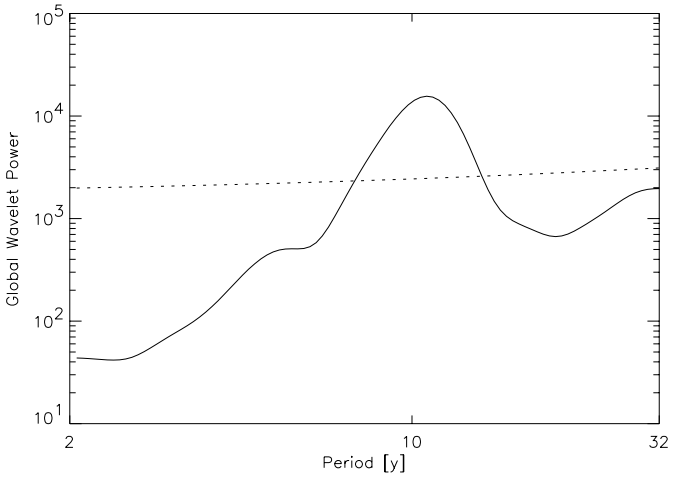

Fig. 5. Global wavelet power spectrum of the Zurich sunspot relative numbers, R_Z. The solar activity exhibits a prominent peak at a mean period of 10.7 years. The 95% confidence level is also plotted (dotted line). It increases with increasing period T due to the higher correlation of neighboring wavelet coefficients for larger scales a, i.e. period T.

the mean value of the first (i.e. highest frequency) scale of the corresponding wavelet power spectrum. Then, an "effective" uncertainty $\sigma_{\rm eff}$ is calculated by summing up the errors of all three factors. Finally, the width of the ridge in the direction of a at one $\sigma_{\rm eff}$ below the maximum. However, the true error is likely to be larger since we do include neither possible systematic measurements errors nor the variable quality of historical records.

The five proxies yield a consistent picture of past solar cycle length variations. They are also compatible with the record given by FL91. From the five direct proxies considered, only $R_{\rm g}$ extends throughout the Maunder Minimum. We were not able to detect any significant and connected cyclic variation during that time, in accordance with Frick et al. (1997) who reported a hardly significant peak around 30 years during the Maunder Minimum. We find some power before the Maunder Minimum which shows a slightly greater mean cycle length than the record of FL91. However, it is well below the 95% confidence level.

5. Analysis of the ^{10}Be record

The analysis of the ^{10}Be record is subject to much larger uncertainties compared to the analysis of direct proxies presented in the previous section. This is due to the fact that the ^{10}Be concentration in ice not only reflects the production rate, which is modulated by the solar activity, but also atmospheric transport and deposition processes (Beer et al. 1994b). In spite of this "noise", i.e. the short-term fluctuations, the 11-y Schwabe cycle is still visible in the Fourier power spectrum plotted in Fig. 7 (Beer et al. 1994a).

We present the wavelet power spectrum of the ^{10}Be record in Fig. 8. The ridge corresponding to the solar activity period is much less pronounced compared to Figs. 3 and 4. There are two epochs around 1500–1600 and 1950, respectively, when there is no unique ridge around 11-years and at least two different

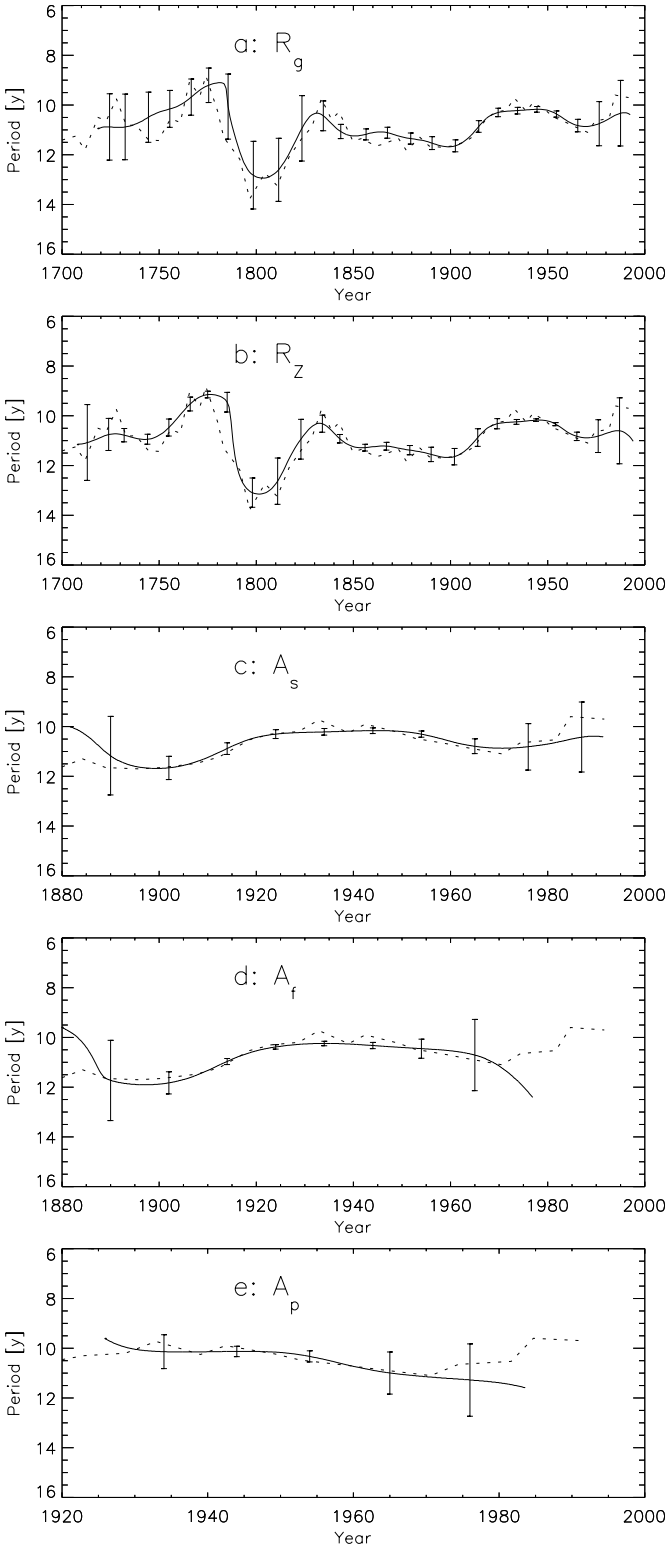

Fig. 6a–e. Variations of the solar cycle length extracted from the five records of direct indicators of solar magnetic activity shown in Figs. 1a–e. The error bars are based on intrinsic noise estimates and do not include possible systematic errors. They increase towards the boundaries of the curves. All curves correlate well and are in good agreement within the error bars. Also plotted as the dotted curve in each frame is the solar cycle length determined by FL91.

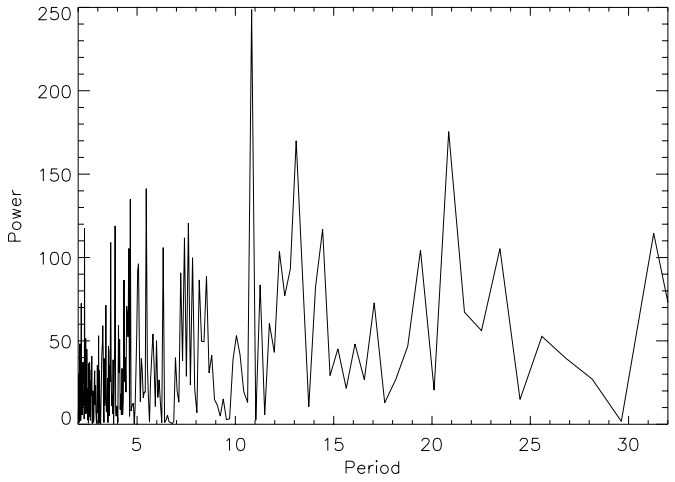

Fig. 7. Fourier power spectrum of the ^{10}Be record from Beer et al. (1994a). The mostly prominent peak corresponds to the solar activity cycle.

solutions of solar cycle length variations are possible. Also, around 1750 there is no significant power at all between 5 and 30 years periods.

Let us now discuss the behavior of the ^{10}Be wavelet power spectrum as a function of time. We distinguish between 4 intervals: 1) the Spörer minimum lasting from approximately 1420 to 1530, 2) the period between the Spörer and the Maunder minima, 3) the Maunder minimum from approximately 1645 to 1700 and 4) the period since the Maunder minimum.

Of particular interest is the strong peak present during the Spörer minimum near 1500. It is the strongest peak exhibited by the ^{10}Be wavelet power and corresponds to a period of 20 years. It is highly significant with 99.95% confidence level. During the time between the Spörer and the Maunder minima two distinct ridges are visible which are about equally strong and correspond to averaged periods of about 11 and 20 years, respectively. A ridge in the 11 year range is clearly visible during the Maunder minimum, suggesting that the solar magnetic field continued its cyclic behavior throughout this period, although no sunspot cycle was visible. The wavelet power is significant at the 95–98% confidence level during that time. Hence, the wavelet power spectrum supports the conclusion reached by Beer at al. (1998) on the basis of a Fourier analysis.

After around 1750, significant power (above the the 80–90% confidence level) is always present. Between approximately 1700 and 1750 the power is relatively weak and there is actually a gap around 1750 when no significant power was present. This behavior is again similar to that observed by Beer et al. (1998).

Evaluation of the global wavelet power spectrum is presented in Fig. 9a. It confirms the presence of two significant peaks at 13.1 and 22.0 years, respectively. The period of ≈13 years is rather long in terms of the solar activity cycle. However, considering its relatively low significance (note that the dotted lines in Fig. 9 are only the 68% confidence level) it is still compatible with the results of Sect. 4.1. These two peaks seem to correspond to the second and third strongest peaks in the Fourier power spectrum plotted in Fig. 7. In order to test whether the peaks are unduly affected by the interval prior to 1700, we have determined the global wavelet power spectrum also between 1700 and the present only. It is plotted in Fig. 9b and can be compared directly with Fig. 5. Now the peak lies at 11.1 years, in better agreement with the direct proxies, although is is very broad.

We apply the same method as described in Sect. 4.1 to extract the solar cycle length variations from the ^{10}Be record. However, if multiple solutions are possible (due to several ridges between 7 and 20 years) we evaluate them separately. The results are presented in Fig. 10. Compared to Fig. 6 the error bars are much larger due to the lower significance of the solar activity ridge in the wavelet power spectrum. Most prominent is, again, the strong dip prior to the Maunder Minimum where the solar cycle length increases to 20–25 years. Just before the Maunder minimum there are two branches of possible cycle length variations. The short period branch is compatible with FL91 and is also more significant. However, it would imply an almost instantaneous jump of the solar cycle length from ≈22 to ≈12 years at around 1560–1570. Around the middle of the 20th century there are also two branches. Of these, the one with the longer period would yield extraordinarily long cycles 17–19, which cannot be found in any of the direct proxy records.

Comparison of the results from the ^{10}Be record with FL91 between 1700 and the present shows less coincidence and a lower fidelity than what has been obtained from the direct proxies. Considerable qualitative agreement was nevertheless found. The two minima around the end of the 18th and 19th centuries and the intervening maximum, respectively, show up in both records and they also agree relatively well during the 20th century if we neglect the long period branch in the ^{10}Be record. Nevertheless, the two curves often differ by more than the statistical errors, in contrast to the results obtained from the other indicators. The presence of multiple branches at certain epochs also makes interpretation of the power spectrum more difficult.

The results of the wavelet technique can be compared to an earlier determination of the cycle length by Beer et al. (1994a). In this approach the instantaneous frequency ("solar melody") was calculated for each data point using the Hilbert transform. The low pass filtered data of Beer et al. (1994a) are plotted in Fig. 11 (dotted line) after applying a binomial filter to adjust the resolution to the one of the wavelet power data. Both curves show considerable agreement especially since the middle of the last century. For earlier times, the correlation is less pronounced although both curves still show qualitatively the same behavior. For example, both curves show the trend towards longer cycles during the 16th century and also a period of longer cycles around the end of the 18th century.

6. A composite cycle-length record

By combining the results of Sect. 4.1 and 5 we can now construct a composite record of solar cycle length variations over almost 600 years, which is plotted in Fig. 12. Since 1700 only the direct solar indicators have been used. The cycle lengths

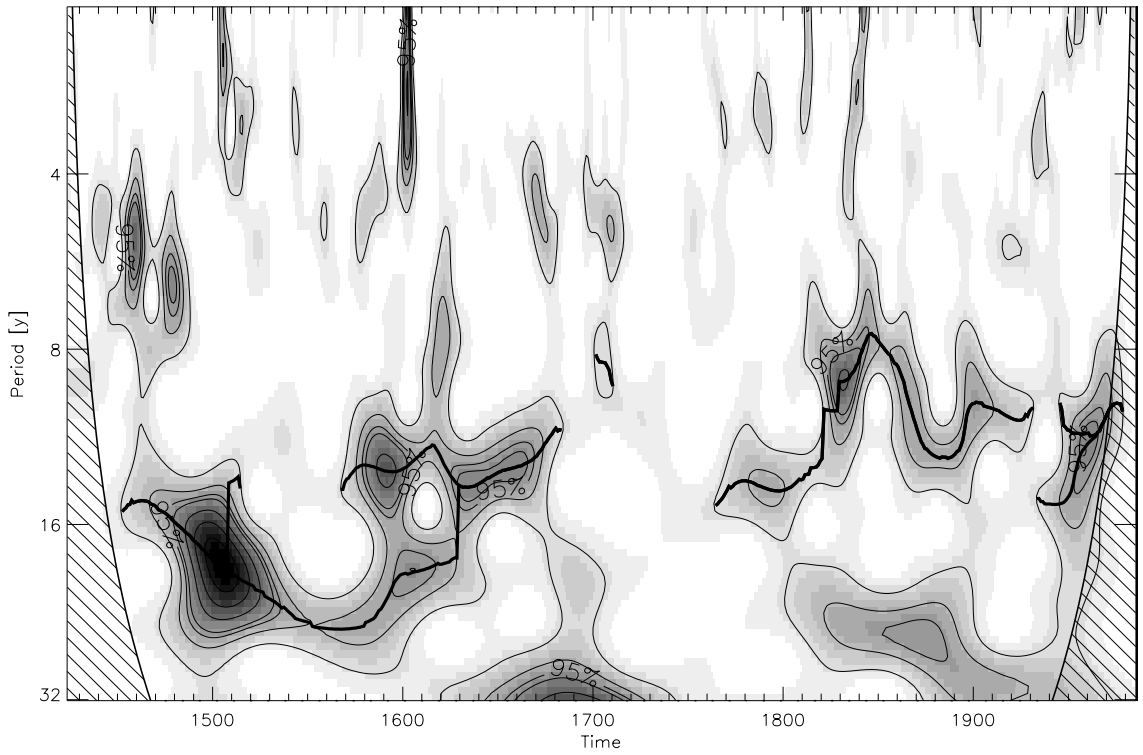

Fig. 8. Wavelet power spectrum of the ^{10}Be record. Although the solar activity signature is only weakly detectable, there is some concentration of power around 11–13 years after 1750 and around 20 years between 1500 and 1600, respectively. The peak around the beginning of the 16th century at a period of about 20 years is the strongest one of the whole wavelet power spectrum. It is highly significant and lies well outside the given DOI.

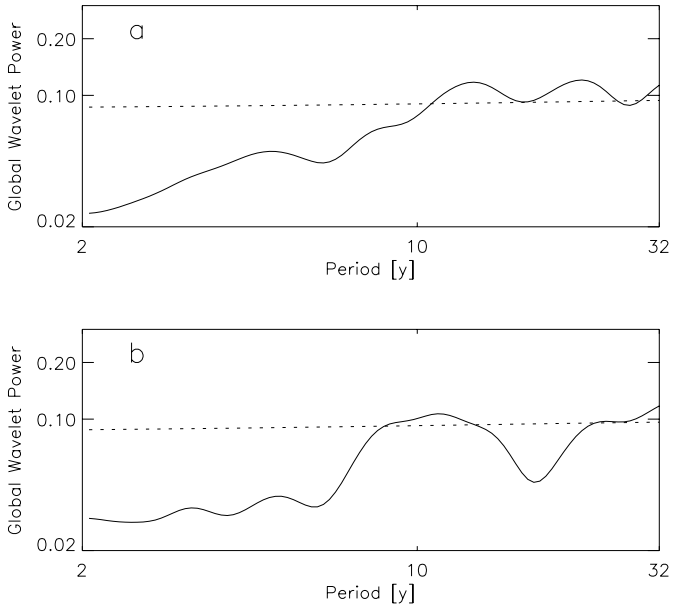

Fig. 9a and b. Global wavelet power spectrum of the ^{10}Be record for the period **a** 1423 to 1985 and **b** 1700 to 1985. The two peaks in frame **a** correspond to periods of 13.1 and 22.0, respectively, and are about equally strong. The latter is mainly caused by the period before the Maunder minimum. If only the time between 1700 and the present is considered (frame **b**) the solar activity period at 11.1 years is pronounced although it is rather broad. The dotted lines mark the 68% confidence level.

from each were weighted by the inverse of the square of the statistical uncertainty (indicated by the error bars in Fig. 6) before combining them. Prior to 1700 only the ^{10}Be record has enough power to extract significant cycle length variations and both of the possible branches are shown.

7. Summary and conclusions

In the present paper we used the continuous wavelet transform to extract information on the length of the solar activity cycle from six different records of solar activity. The curves obtained from the five direct indicators of solar activity (sunspot relative number, group sunspot number, sunspot area, facular area and Ca plage area) are in good agreement with each other and with the cycle length record originally proposed by FL91 (which they obtained by carrying out a 1-2-2-2-1 smoothing; Lassen & Friis-Christensen, 1995). The agreement with the unsmoothed cycle-length record of Kelly & Wigley (1992) is smaller. Since the FL91 curve correlates far better with northern hemisphere air temperature records than the Kelly & Wigley cycle lengths this results lends further weight to the conclusion of FL91 that the Sun effects the Earth's climate. Using concentrations of cosmogenic ^{10}Be we have extended the cycle length record further into the past. This part of the record, before 1700, is significantly less reliable, however. To further confirm the remarkable relation between the solar cycle length and indicators of terrestrial

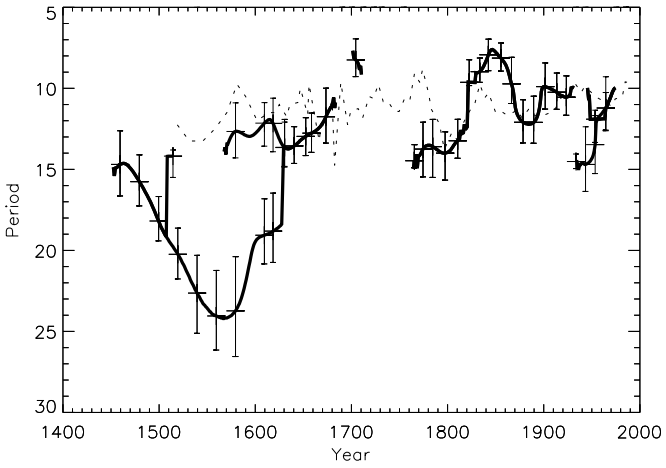

Fig. 10. Extraction of solar cycle length variations from the ^{10}Be record. Most prominent is a strong increase of the cycle length between the Spörer and the Maunder minima. During the end of the 16th and the beginning of the 17th century as well as during the middle of the 20th century two different cycle length extractions are allowed by the data. Again, the record of FL91 is given by the dotted line.

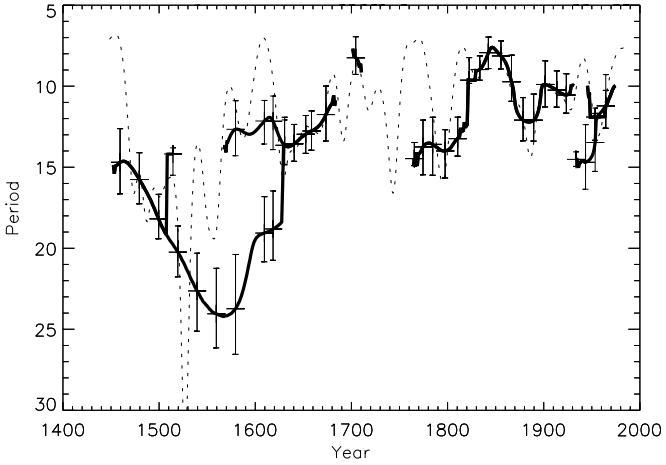

Fig. 11. Comparison of past solar cycle length variations as derived from the wavelet power spectrum and from the "solar melody" (Beer et al. 1994a). Both curves correlate rather well for the last two centuries and show the trend towards longer cycle lengths during the 16th century.

climate it would be necessary to have longer and more reliable time-series.

Additional cosmogenic isotope records from different sites will help to reduce the local transport component and to improve the signal to noise ratio. The time resolution for ^{10}Be records is limited to the mean atmospheric residence time of about 1–2 years. However, provided a high quality ice core with a very precise time scale is available, the analysis of solar cycles can be extended to at least 10'000 years. Such work with somewhat lower time resolution is in progress.

Acknowledgements. We thank Reto Knaack for helping with the analysis and the referee Dr. Anne Vigouroux for many helpful comments. This work was supported by the Swiss Nationalfonds under NF grant No. 2000-046894.96.

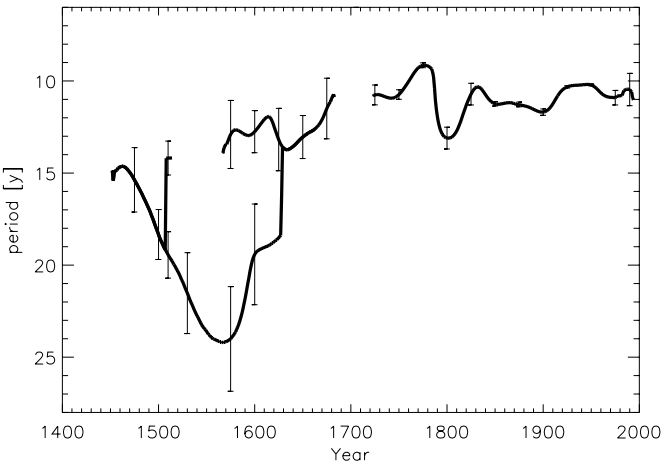

Fig. 12. Composite of the length of the solar activity cycle based on the indicators of solar activity analyzed in the present paper.

References

Baliunas S., Soon W., 1995, ApJ 450, 896
Beer J., Tobias S., Weiss N., 1998, Solar. Phys. 181, 237
Beer J., Blinov A., Bonani G., et al., 1990, Nat 347, 164
Beer J., Baumgartner St., Dittrich-Hannen B., et al., 1994a, In: Pap J., Fröhlich C., Hudson H.S., Solanki S.K. (eds.) The Sun as a Variable Star: Solar and Stellar Irradiance Variations. Cambridge University Press, Cambridge, IAU Coll.143, 291
Beer J., Joos F., Lukasczyk Ch., et al., 1994b, NATO ASI Series I 25, 221
Bocchialini K., Baudin F., 1995, A&A 299, 893
Chui C.K., 1992, An Introduction to Wavelets. Academic Press, Boston
Delpart N., et al., 1992, IEEE Trans. of Information Theory 38, 644
Fligge M., Solanki S.K., 1997, Solar Phys. 173, 427
Foukal P., 1996, Geophys. Res. Lett. 23, 2169
Frick P., Galyagin D., Hoyt D.V., et al., 1997, A&A 328, 670
Friis-Christensen E., Lassen K., 1991, Sci 254, 698
Goupil M.J., Auvergne M., Baglin A., 1991, A&A 250, 89
Goupillaud P., Grossmann A., Morlet J., 1984, Geoexploration 23, 85
Grossmann A., Kronland-Martinet R., Morlet J., 1993, In: Combes J.M., Grossmann A., Tchamitchian Ph. (eds.) Wavelets, Time-Frequency Methods and Phase Space. Springer-Verlag, 2
Grossmann A., Morlet J., 1984, SIAM J. Math. Anal. 15, 737
Hjorth P.G., Villemoes L.F., Teuber J., Florentin-Nielsen R., 1992, A&A 255, L20
Hoyt D.V., Schatten K.H., Nesmes-Ribes E., 1994,Geophys. Res. Lett. 21, 2067
Hoyt D.V., Schatten K.H., 1998, Solar Phys. 179, 189
Kelly P.M., Wigley T.M.L., 1992, Nat 360, 328
Lassen K., Friis-Christensen E., 1995, J. Atmos. Terr. Phys. 57, 835
Meyers S.D, Kelly B.G., O'Brien J.J., 1993, Mon. Wea. Rev. 121, 2858
Ochadlick A.R. Jr., Kritikos H.N., Giegengack R., 1993, Geophys. Res. Lett. 20, 1471
Starck J.L., Bijaoui A., 1994, Signal Processing 35, 195
Starck J.L., Murtagh F., Bijaoui A., 1995, In: Shaw R.A., Payne H.E., Hayes J.J.E (eds.) Astronomical Data Analysis Software and Systems IV, ASP Conference Series, 77
Torrence Ch., Compo G.P., 1998, Bulletin of the American Meteorological Society 79, 61
Vigouroux A., Delache Ph., 1993, A&A 278, 607
Vigouroux A., Delache Ph., 1994, Solar Phys. 152, 267